

# Shear zones in granular media: 3D Contact Dynamics simulation

Alexander Ries and Dietrich E. Wolf

*Department of Physics, University Duisburg-Essen, D-47048 Duisburg, Germany*

Tamás Unger

*Department of Theoretical Physics, Budapest University of Technology and Economics, H-1111 Budapest, Hungary*

(Dated: November 19, 2018)

Shear zone formation is investigated in slow 3D shear flows. We simulate the linear version of the split-bottom shear cell. It is shown that the same type of wide shear zones is achieved in the presence as well as in the absence of gravity. We investigate the relaxation of the material towards a stationary flow and analyze the stress and the velocity fields. We provide the functional form of the widening of the shear zone inside the bulk. We discuss the growth of the region where the material is in critical state. It is found that the growth of the critical zone is responsible for the initial transient of the shear zone.

PACS numbers: 47.57.Gc, 45.70.-n, 83.50.Ax

## I. INTRODUCTION

Granular materials consist of macroscopic grains which have simple interactions and obey the laws of classical mechanics. The resulting behavior, however, can be surprisingly complex. This is shown by a large variety of phenomena [1, 2] which, in most cases, present great challenges to theoretical descriptions.

In the present paper we focus on one of the unsettled problems of granular media: the quasi-static rheology [3]. The flow is called quasi-static when inertia effects are negligible. This can be achieved by a combination of large pressure and low deformation rate.

An important property observed for this type of flows is that stresses become independent of the deformation rate. This is remarkable because it is the rate dependence that is naturally expected to be responsible for the rheology. For quasi-static flows the link between stress and deformation rate is missing and we lack the constitutive law which could describe the deformation field in the material.

An experimental setup which is particularly suited to provide insight into quasi-static granular flow is the split-bottom shear cell. It has recently been the subject of many experimental, theoretical and simulational studies [4, 5, 6, 7, 8, 9, 10, 11, 12, 13]. In experiments the cell has cylindrical form called the modified Couette cell [5]. It is a container whose bottom is divided into a central disk and an outer ring. The disk rotates slowly with respect to the rest of the container. When sand is filled in, it is dragged along by the rotating central bottom disk so that a shear zone emerges in the material, where the shear deformation is localized. It starts at the perimeter of the bottom disk, spreads into the bulk and reaches the top surface, if the filling height is not too large. The shear zone can be characterized by its central sheet (the sheet of the maximum shear rates) and the width of the zone around the central sheet.

Depending on the experimental conditions the behavior of the central sheet can be quite complicated. Due to

the cylindrical shearing it gets a nontrivial curved shape with decreasing radius towards the top of the system. The shape depends strongly on the filling height [5]. For large  $H_{\text{fill}}$  the central sheet even detaches from the top and dives entirely into the bulk [7, 8, 9] forming a cupola-like shape. If two materials are used, the central sheet can be refracted, when the shear zone leaves one material and enters into the other [12]. All these effects will be avoided hereafter in the paper. We deal with the linear version of the split-bottom cell (see later) [10, 11], where the central sheet remains a vertical plane. Therefore the flow becomes simpler and widening of the shear zone can be analyzed more easily.

The width of the shear zone  $W$  has been found to be an increasing function of the bulk height  $z$  and also an increasing function of the filling height  $H_{\text{fill}}$  [5, 9, 13]. The width at the top ( $W_{\text{top}}$ ) grows more slowly than the filling height but faster than the square root of  $H_{\text{fill}}$ . The experimental data suggest that  $W_{\text{top}}$  is approximately a power law with exponent  $2/3$  [5, 8].

Although it is a very basic question, where this type of rheology comes from, no satisfying description has been found so far. There are proposals what the governing mechanism of shear zones could be. Some of these theoretical approaches [7, 10, 11, 13] are reassuring in the sense that they lead to wide shear zones and, at the same time, satisfy the condition of rate independence. One approach [7, 12, 13] is based on the weakest sliding surface which fluctuates during the flow, another one [10, 11] is based on the variation of the effective friction coefficient depending on the orientation of the local shear plane. At the current stage these models are not very well established and concerning the details they leave many questions open.

It is hard to refine existing models or propose new candidates because not enough details are known about the flow. Especially, precise data are needed that are measured in the bulk, regarding e.g. velocity and stress fields.

With our present study we provide some new details about the flow in the split-bottom shear cell. We per-

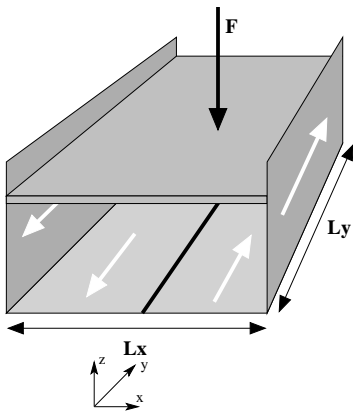


FIG. 1: The linear split-bottom cell.

form DEM simulations where the velocities and stresses are easily accessible in the bulk. Previous experiments and simulations were in gravity which leads to an inhomogeneous pressure distribution. We analyze shear zone formation also in a zero gravity environment in order to clarify the role of gravity.

## II. DESCRIPTION OF THE NUMERICAL EXPERIMENT

In our simulations we examine a linear version of the split-bottom shear cell [10, 11] shown in Fig. 1. Here the bottom is cut along a straight line. The left and the right sides of the boundary move along the  $y$  axis in opposite directions both with velocity  $v_{\text{shear}}$ . In  $y$ -direction periodic boundary conditions are applied. Small grains are glued to the side walls and to the bottom in order to make their surface rough.

We have a frictionless piston on the top of the system. Its position in  $z$ -direction gives the filling height of the system. The piston has a compressing force  $F_{\text{pist}}$  on it acting in negative  $z$ -direction. We use two ways to put the system under pressure. Either we apply a large force  $F_{\text{pist}}$  and set gravity to zero or we use gravity instead and put only a weak force on the piston. The role of the piston in the former case is to provide the confining pressure on the system. In the latter case it keeps only the top surface flat and ensures a constant filling height for the whole system. Then the piston has negligible effect on the pressure distribution in the bulk which is generated essentially by gravity.

Our simulations are discrete element simulations based on the method of contact dynamics [14, 15]. The grains are noncohesive, rigid and spherical interacting via frictional contact forces. The value of the friction coefficient is set to 0.2. Throughout this paper every length is measured in units of the maximum grain radius. Radii are uniformly distributed between 0.8 and 1.0.

We tested various system sizes. The number of the grains  $N$  contained by the shear cell varies between 1 000

and 100 000. The width  $L_x$ , the length  $L_y$  and the filling height  $H_{\text{fill}}$  of the systems range from 20 to 240, from 12.5 to 75, and from 8 to 70, respectively.

Our simulation corresponds to an experimental situation where the grains have density  $2400 \text{ kg/m}^3$  and maximum radius  $1 \text{ mm}$ . The value of  $v_{\text{shear}}$  is set to  $0.7 \text{ cm/s}$  (unless stated otherwise). The force  $F_{\text{pist}}$  is chosen proportional to the surface of the piston in order to maintain the same pressure. This pressure is  $500 \text{ N/m}^2$  when gravity is switched off. Together with gravity the pressure on the piston is set to  $25 \text{ N/m}^2$ .

The preparation of the system starts from a gas state where grains have random positions. First we compactify the material with the piston then gravity is switched on if needed and the shearing starts. Before measuring velocities and stresses we let the system relax in order to reach stationary flow.

## III. RESULTS

### A. Orthogonal velocities

First we examine whether the shear cell generates any convection orthogonal to the shear direction  $y$ . The components of the coarse-grained velocities  $v_x$ ,  $v_y$  and  $v_z$  are functions of the coordinates  $x$  and  $z$  (the coordinate  $y$  is averaged out). In the present shear cell  $v_x$  and  $v_z$  would vanish for a laminar flow of a Newtonian fluid, however, this does not hold a priori for quasi-static flow of granular media. One could imagine various kinds of stationary flows with non-vanishing convection in  $x$ - $z$ -plane, e.g., where grains, besides moving in  $\pm y$ -direction, slowly rise near to the symmetry plane and descend far away from it.

Fig. 2 shows a typical orthogonal velocity field. This simulation contains 100000 grains and is performed without gravity. Before recording velocity data we sheared the system for a long time in order to achieve a steady state. During this preshearing the system had total shear displacement  $\lambda = 500$  (this is the displacement of the two sides of the shear cell with respect to each other). The velocities shown in Fig. 2.a are obtained by an average over a further shear displacement 60. This velocity field seems to be merely random fluctuation where vortices arise due to mass conservation. The largest velocities are located near the symmetry plane of the cell and their magnitude is about 200 times smaller than the shear velocity of the cell. These velocities decrease further if the average is taken over larger shear displacements. This is shown in Fig. 2.b where the shear displacement is 5 times larger compared to Fig. 2.a. Thus we find no convection orthogonal to the shear direction. If such convection is induced by the shearing then it must be at least 4 orders of magnitude smaller than the shear velocity itself.

In the followings we will focus on the motion along the shear direction  $y$ .

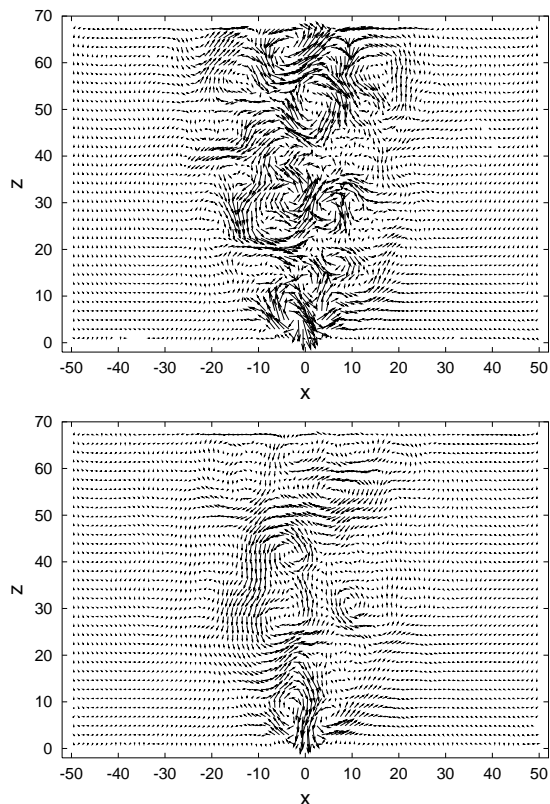


FIG. 2: The average velocity field in the cross section of the cell orthogonal to the shear direction. The time average is taken over a shear displacement 60 for (a) and 300 for (b).

### B. Velocity profiles

The shear flows found in our simulations are in agreement with previous experimental and numerical measurements in the modified Couette cell [4, 5, 8, 9, 11]. Our new results concern the slow evolution in the outskirts of the shear zone, its widening with increasing distance from the bottom slit (Sec. C), and the influence of gravity (Sec. D). In particular it will be shown that gravity has surprisingly little effect on the properties of the shear zone.

In order to examine the velocities  $v_y$  we divide our system into different slices at constant heights  $z$ .  $z$  ranges from zero to the filling height  $H_{\text{fill}}$ . At each height  $z$  the velocity  $v_y$  goes from  $-v_{\text{shear}}$  to  $v_{\text{shear}}$  as  $x$  is increased. This transition is very sharp at the bottom, where the boundary condition prescribes a step function, and broader towards the top of the system. Fig. 3 shows the profiles for a system without gravity in several heights.

The velocity profiles can be well fitted with error functions [5]. Consequently, the shear rate  $\dot{\gamma}_{xy}$  as a function of  $x$  is a Gaussian curve. We define the *width of the shear zone*  $W(z)$  as the square root of the second moment of the (normalized) shear rate at height  $z$  thus the width of the zone equals to the width of the corresponding Gaus-

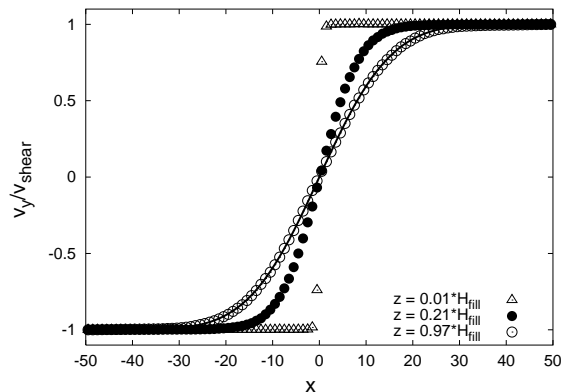


FIG. 3: The velocity profiles are taken from the same system at three different heights  $z$ . The line shows an error function fit.

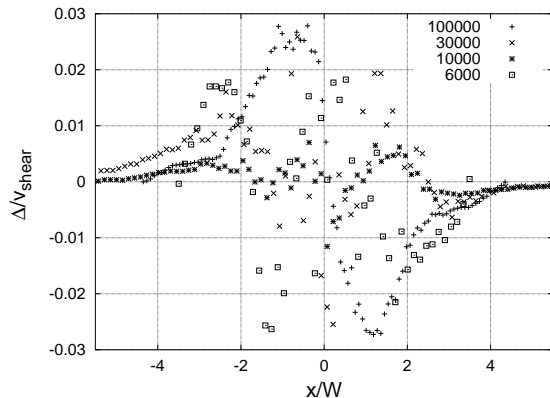


FIG. 4: The difference  $\Delta$  between the velocity data and the fit by error function is shown. The data are recorded in nine different systems. Total number of grains used in the simulations are between 6 000 and 100 000. Minimum and maximum heights are 25.6 and 69. In all cases shown here gravity is set to zero. Only the fits of the velocity profiles at  $z = H_{\text{fill}}$  are evaluated. For each system the coordinate  $x$  is normalized by the width of the shear zone measured in the top layer.

sian curve.

The accuracy of the fit by an error function is assessed in Figures 4 and 5. In Fig. 4 the deviations between data and fit are plotted for several systems. Deviations are random and approximately 2% of  $v_{\text{shear}}$  near the center. Further away from the center the errors become smaller, however, systematic deviations can be seen: They are positive on the left and negative on the right hand side. From Fig. 5 one can conclude that these systematic deviations are going to vanish, if one lets the simulations run longer. The velocity profile approaches the error function shape first in the center, but much more slowly in the outskirts. If we let the simulations go on, the tail of the velocity profile keeps evolving and is getting closer and closer to the Gaussian tail of the error function. We will come back to the relaxation process in section III F.

The above properties of the velocity distribution are

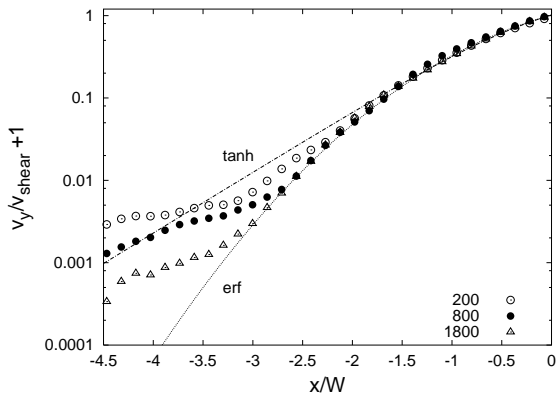


FIG. 5: Slow time evolution of the tail of the velocity profile is shown for a system of 10 000 grains at the filling height  $H_{\text{fill}} = 25.6$ . For the three different profiles the measurements are started at shear displacement 200, 800 and 1800. Each profile represents an average over an additional shear displacement 200. The two lines are fit curves of the velocity data: the upper one is a hyperbolic tangent, the lower one is the error function. It can be seen that the velocities follow the Gaussian tail of the error function the better the larger the shear deformation of the sample is.

in agreement with experimental data [5] which have been achieved in gravity in a modified Couette cell, whereas the simulation data presented in Figs. 3, 4 and 5 were obtained for zero gravity. As we will discuss below, gravity has indeed only very little influence on the velocity profile.

### C. Widening of the shear zone in the bulk

Previous experimental and numerical studies revealed that the shear zone becomes wider as it goes from the bottom  $z = 0$  towards the top  $z = H_{\text{fill}}$ . There are some experimental and theoretical indications reported in [10] that  $W(z)$  may be a power law with exponent between 0.2 and 0.5. However, we are not aware of any conclusive experimental data concerning the exact shape of the function  $W(z)$ . It is a crucial question what the functional form is because it provides a very strong test for theories. Such tests are clearly needed as the problem of quasi-static flow and shear zone formation is far from understood. This field is in the stage of searching for candidates of models in order to gain a better understanding of basic phenomena.

It is a nice feature of computer simulations that one can easily access the velocity data also inside the bulk. Based on these data we are able to deduce the functional form of  $W(z)$ . We tested many systems with different filling heights. It turns out that all the width data collapse if plotted in the frame  $(W(z)/W_{\text{top}}, z/H_{\text{fill}})$ . The collapse of the data can be seen in Fig. 6. The master curve that

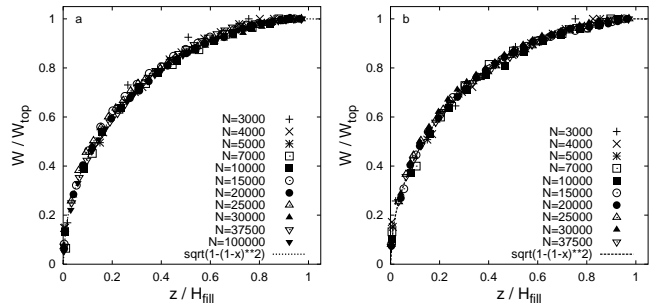


FIG. 6: Data collapse of width - bulk height data is achieved when rescaled with the maximum width and the filling height, respectively. Systems containing different number of grains  $N$  are plotted here. Filling heights ranges from 9 to 69. a) without gravity, b) with gravity.

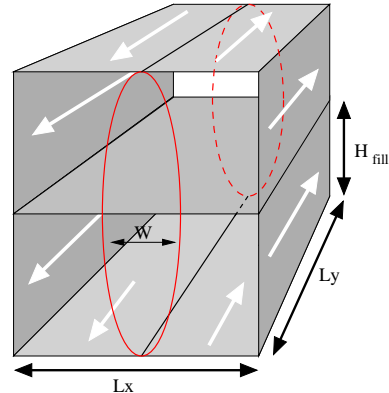


FIG. 7: The system and its mirrored counterpart above.

the data follow is a quarter of a circle:

$$W(z) = W_{\text{top}} \sqrt{1 - \left(1 - \frac{z}{H_{\text{fill}}}\right)^2}. \quad (1)$$

Thus we find that the widening of the shear zone starts with an exponent 1/2 for small values of  $z$  but soon departs from the power law.  $W(z)$  hits the top of the system at a right angle.

This latter condition of the right angle seems to be quite reasonable at least for the case when gravity is switched off. The frictionless piston we apply at the top exerts no drag force on the material, but only applies normal pressure on the system. An equivalent situation can be achieved if we take the original system together with its mirror image (see Fig. 7) and at the same time we leave the piston away. Then we have a split boundary both at the bottom and at the top. The total height of the system is then two times the original filling height. For symmetry reasons there is no drag force between the upper and lower parts of the system which explains the equivalence. And again for symmetry reasons the curve  $W(z)$  must be perpendicular to the plane of the removed piston.

Interestingly the presence or absence of gravity has no

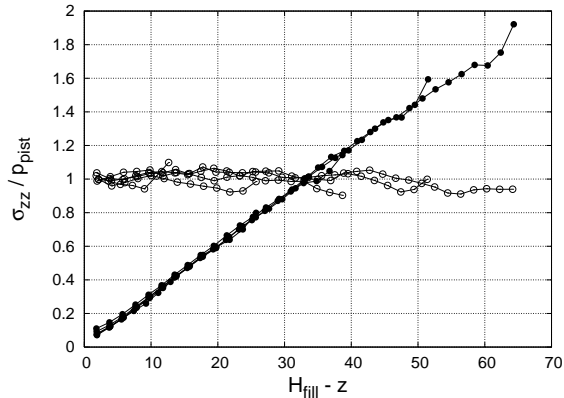


FIG. 8: The stress  $\sigma_{zz}$  as the function of depth. Full circles are recorded in gravity while open circles correspond to zero gravity where the entire pressure is provided by a piston. For each case we plot 4 different curves which represent different number of grains filled in the shear cell ( $N$ : 5000, 10000, 15000, 20000 and 25000). The filling height  $H_{\text{fill}}$  changes proportionally to  $N$ . In gravity  $\sigma_{zz}$  corresponds to hydrostatic pressure.  $p_{\text{pist}}$  is the pressure on the piston in zero gravity.

influence on the data collapse: the master curve given by Eq. 1 is valid for both cases (Fig. 6).

#### D. Role of gravity

Significant efforts have been made recently to understand the behavior of wide shear zones. However, all experimental, theoretical and numerical studies subjected to split bottom shear cells (either linear or cylindrical cells) [4, 5, 6, 7, 8, 9, 10, 11, 13] investigated shear zones under gravity.

Gravity leads to an inhomogeneous stress distribution in the system. Stresses even go to zero as the free surface of the sample is approached. It is not unplausible to imagine that gravity might be responsible for certain features of the shear zones (e.g. their widening towards the free surface).

In Fig. 8 we show the stress component  $\sigma_{zz}$  at the symmetry plane of the shear cell. It can be seen that  $\sigma_{zz}$  is proportional to the depth in case of gravity and approximately constant without gravity.

Recently, Depken et al. [10, 11] argued that in the quasi-static regime one cannot achieve wide shear zones, if the effective friction coefficient  $\mu_{\text{eff}}$  is assumed to be constant. For constant  $\mu_{\text{eff}}$  the shear zone should localize to a thin layer. In their model the widening of the shear zone is attributed to the dependence of  $\mu_{\text{eff}}$  on the angle  $\Theta$  between the direction of gravity and the local tangent plane of the constant velocity surfaces. (In other words they assumed that the frictional properties of the material depend on the orientation of gravity with respect to the local sliding plane.)

Our simulation data do not support the above picture. The effective friction  $\mu_{\text{eff}}$  might vary throughout

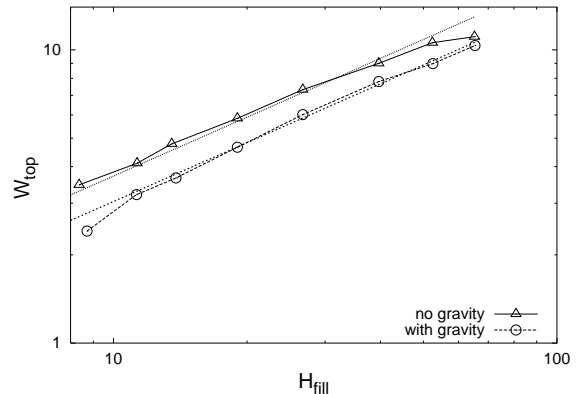


FIG. 9: Width of the shear zone at the top of the systems plotted as function of the filling height. Gravity reduces the width of the shear zones. Lines are not fits, they only show the slope of exponent  $2/3$ .

the shear zone, however, the direction of gravity does not seem to play any important role here. As we discussed in previous sections the velocity profiles are qualitatively the same no matter whether gravity is present or not. Surprisingly, body forces or decreasing pressure are not needed for wide shear zones.

In fact, shear zones exhibit even larger width when gravity is switched off. The width gets larger by a factor  $1.2 \pm 0.1$ . This can be seen in Fig. 9 where the top width of the shear zone for various filling heights is plotted.

Why gravity contracts the shear zone can be explained by the pressure distribution. At the bottom the pressure, and thus also the frictional forces, are much stronger than at the top of the system. Therefore the rheology is dominated by the lower part of the system. Compared to the case of homogeneous pressure this acts as if the system had effectively smaller filling height which leads to a smaller width of the shear zone. The contracting effect of gravity is also discussed in [16] based on the principle of minimum energy dissipation.

The experimental data of Fenistein et al. [5, 8] showed that  $W_{\text{top}}(H_{\text{fill}})$  is approximately a power law with exponent  $2/3$ .  $W_{\text{top}}(H_{\text{fill}})$  found in our simulations is shown in a log-log plot in Fig. 9, where the exponent  $2/3$  is also indicated for comparison. The data follow approximately the experimental behavior. For a precision value of the exponent or a discussion of deviations from a power law better statistics is needed, however.

#### E. Influence of additional parameters

It was assumed so far that the flow is quasi-static, i.e. the shear velocity  $v_{\text{shear}}$  is small enough that no rate-dependence is observed in the behavior of the shear zone. We also intended to choose the width  $L_x$  and length  $L_y$  of the systems large enough in order to exclude their influence on the flow. Furthermore, it was assumed that

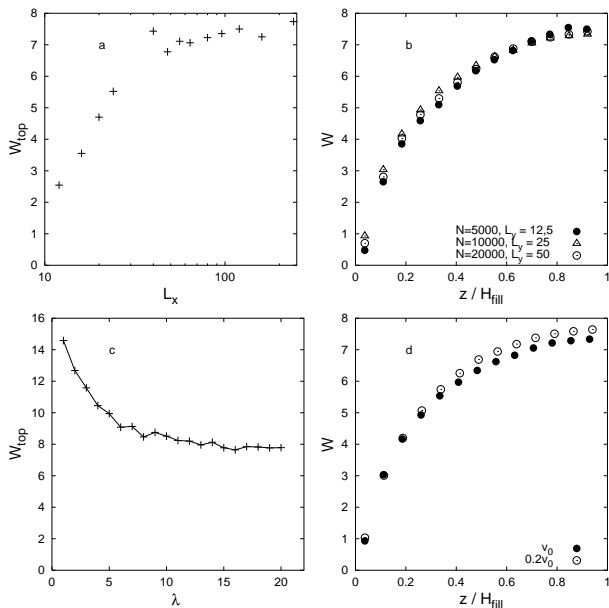


FIG. 10: Robustness of the width of the shear zone. a) The effect of the system width  $L_x$  on the top width of the shear zone. b) The width of the shear zone is plotted as function of the bulk height  $z$  for three different lengths  $L_y$  of the shear cell. c) Relaxation of the top width as function of the shear displacement  $\lambda$ . d) The influence of the shear velocity  $v_{\text{shear}}$  on the curve  $W(z)$ . Full circles denote five times larger shear velocity than the open circles.

the analysis of the shear zone was taken after initial transients in the stationary flow regime, i.e. the total shear displacement  $\lambda$  was large enough to ensure complete relaxation.

In this section we check the influence of the parameters  $L_x$ ,  $L_y$ ,  $\lambda$  and  $v_{\text{shear}}$  to show that they are chosen properly and do not alter the properties of the shear zone. For this purpose we take one of the previous samples as reference system and demonstrate the role of the four parameters there. The reference system contains  $N = 10000$  grains, has the size  $L_x = 80$ ,  $L_y = 25$ ,  $H_{\text{fill}} = 25.6$  (this system appeared already in Figures 4, 5, 6 and 9).

First we vary the width of the system  $L_x$  and the number of grains  $N$  proportionally to  $L_x$  in order to maintain the same filling height. Other parameters are constant. The effect on the width of the shear zone can be seen in Fig. 10.a. Around the reference point  $L_x = 80$  the width remains constant. The shear zone “feels” the effect of the side walls only if  $L_x$  drops below 40 where the shear zone can be strongly contracted by lowering  $L_x$ .

For the parameter  $L_y$  we test values 12.5, 25 and 50 (again  $N$  is changed proportionally) while other parameters are constant. Fig. 10.b shows that the width of the shear zone remains essentially the same (changes are small and without systematics).

In order to avoid initial transients all the systems presented in this paper undergo a preshearing over a total displacement of more than  $\lambda > 60$ , and only after that

we start collecting data. Fig. 10.c shows that the transient period is indeed completed during the preshearing: The width of the shear zone becomes independent of the displacement  $\lambda$ . The origin of the initial transient is discussed in Sec. III F.

Due to the larger time resolution applied here velocity fluctuations become also larger. In order to improve the statistics 20 parallel simulations were taken. In each case the system had the same macroscopic parameters as our reference system. In Fig. 10.c the time evolution of  $W_{\text{top}}$  was achieved by ensemble average over the 20 simulations.

Next we turn to  $v_{\text{shear}}$ . If pressure conditions are the same it depends on the speed of driving whether the flow is quasi-static. For relative large driving speeds, but still in the dense flow regime, inertia effects come into play which weaken shear localization and results in wider shear zones. Then the width of the shear zone can be made smaller by lowering the driving speed. But if the driving gets slow enough the rheology becomes independent of the driving rate and the shear zone reaches its minimum width. We test the effect of the driving rate in our reference system by taking five times smaller shear velocity. The new bulk-width of the shear zone is compared with the original one in Fig. 10.d. The data show no further decrease of the width. The width for the reduced driving is even slightly larger due to random fluctuations. Within the accuracy of our numerical measurement the two curves can be regarded as equal.

## F. Shear zone versus critical zone

The shear zone is the region where the major part of the shear deformation takes place. It is described by the function  $W(z)$ . The material, however, is not solid outside the shear zone either. Split-bottom cells fluidize the material everywhere, however the shear rate becomes many orders of magnitude smaller far from the shear zone.

In this section we would like to discuss the concept of the critical state. It has not got any attention so far in the context of the split-bottom shear cells, although, it leads to the emergence of a relevant and new type of zone.

It is known that the mechanical properties of granular media are influenced strongly by the preparation. If one starts shearing a packing the behavior can be different depending on the initial state (density, structure of the contact network, etc): It can lead to different stress responses, effective frictions, dilation or contraction, etc. However, if the material experiences large enough local strain it reaches a unique state regardless of the preparation history. This is the critical state [17, 18, 19, 20, 21] where the material organizes and maintains its microscopic inner structure on shearing. After the critical state has been reached unlimited shear deformation can occur without changes of stresses or density. The characteris-

tic deformation scale needed to erase the memory of the material and reach the critical state is typically around  $\gamma = 0.2$ , where  $\gamma$  is the cumulative shear strain.

Before the shearing starts in the split-bottom cell the fabric of the material reflects the direction of the initial compression or gravity. With the shear deformation this structure is destroyed and new contacts are created against the direction of the shear. This gives rise to strain hardening: the resistance of the material against shear is increased. This does not happen simultaneously all over the sample. When regions in the middle of the shear cell are already in the critical state, regions far away can still be frozen in the initial configuration.

At the beginning, the zone of the critical state starts growing from the split line at the bottom. It reaches quickly the top of the system and also spreads sideways. As the shear rate is very small far from the symmetry plane, the growth of the critical zone becomes extremely slow here. In that sense a steady state can not be reached in the whole system. One expects the flow to become stationary only inside the critical zone.

The growth of the critical zone comes into sight in Fig. 5. The velocity of a given point in the system reaches its final value only after the region becomes critical. The position where the velocity data depart from the stationary curve mark the border of the critical zone. The different velocity profiles recorded in different stages of the simulation show how the width of the critical zone is increasing with time. It can be attributed to the strain hardening why the shear rate is reduced at a given position after it becomes critical.

The reduction of the shear rate due to strain hardening also explains the relaxation of the shear zone that is shown in Fig. 10.c. In the early stage of the simulation where the critical zone is smaller than the shear zone the shear rate is slightly enhanced outside the critical region. This makes the shear zone wider a little bit. After the whole shear zone becomes critical this additional widening effect ceases, and  $W_{\text{top}}$  is reduced to its final value.

According to this interpretation the initial transient of the shear zone is due the time evolution of the critical region. One can estimate the shear displacement  $\lambda$  that corresponds to the transient period by matching the size of the stationary shear zone and the growing critical zone. Using the stationary velocity profile and the cutoff shear strain  $\gamma = 0.2$  one gets  $\lambda = 7.7$  for the transient. This is in excellent agreement with the relaxation observed in Fig. 10.c.

The growth of the critical zone and the transient of the shear zone can be reproduced within the framework of a simple lattice model [16] developed for quasi-static shear flows.

The presence of the critical zone can be observed also in the stress field. The next section is subjected to this question.

## G. Stresses

As the average local velocities have only a  $y$ -component and the system is translational invariant in  $y$ -direction, the local strain rate in the  $(x, y, z)$ -frame has the form

$$\frac{1}{2} \begin{pmatrix} 0 & \frac{\partial v_y}{\partial x} & 0 \\ \frac{\partial v_y}{\partial x} & 0 & \frac{\partial v_y}{\partial z} \\ 0 & \frac{\partial v_y}{\partial z} & 0 \end{pmatrix}. \quad (2)$$

By means of a rotation around the  $y$ -axis a new local frame  $(u, y, v)$  can be chosen in which the strain rate is

$$\frac{1}{2} \begin{pmatrix} 0 & \frac{\partial v_y}{\partial u} & 0 \\ \frac{\partial v_y}{\partial u} & 0 & 0 \\ 0 & 0 & 0 \end{pmatrix}. \quad (3)$$

If initial conditions are forgotten in the critical state (also called steady state flow), stress and fabric tensors are expected to have the same principal axes as the strain rate tensor. Then the stress tensor must have the form [10]

$$\begin{pmatrix} \sigma_{uu} & \sigma_{uy} & \sigma_{uv} \\ \sigma_{yu} & \sigma_{yy} & \sigma_{yv} \\ \sigma_{vu} & \sigma_{vy} & \sigma_{vv} \end{pmatrix} = \begin{pmatrix} P & \tau & 0 \\ \tau & P & 0 \\ 0 & 0 & P' \end{pmatrix}. \quad (4)$$

Depken et al. [11] tested stresses in the linear split bottom cell by soft particle molecular dynamics simulations. They found the expected behavior in the middle part of the cell where stress and strain tensor were co-linear and stresses took the form (4).

However, if the material still remembers its initial structure the alignment of stress and strain is not necessarily valid. Therefore we determine a second local frame  $(u', y, v')$  from the condition  $\sigma_{yv'} = \sigma_{v'y} = 0$  and evaluate the angle  $\alpha$  between the two directions  $(u, v)$  and  $(u', v')$  in the  $(x, z)$ -plane. The lower part of Fig. 11 shows indeed that the angle  $\alpha$  approaches 0 for large shear deformations  $\gamma$ , while the principal directions of stress and strain rate tensor differ during the transient. Correspondingly,  $\sigma_{u'v'}$  approaches 0 for large shear deformations (see Fig. 12), as predicted by Eq.4.

Our numerical test was based on another method than the one used by Depken et al. [11], the contact dynamics algorithm [14, 15], and we used slightly different conditions (zero gravity, piston). Nonetheless, we found the same behavior for regions where the material experienced large shear deformation. Here stress and strain tensors align and the stress corresponds to the reduced form in Eq. 4.

Stress data recorded in a system of 100 000 grains with total shear displacement 820 are presented here as the function of the cumulative local shear strain  $\gamma$ . Fig. 11 shows stress ratios  $\sigma_{yy}/\sigma_{u'u'}$  and  $\sigma_{v'v'}/\sigma_{u'u'}$ . In the critical zone  $\sigma_{u'u'}$  and  $\sigma_{yy}$  are indeed the same and the value  $\sigma_{v'v'}$  is about 10% smaller.

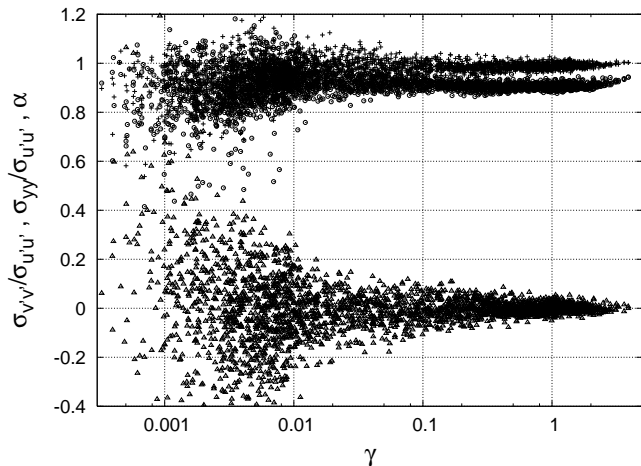


FIG. 11: The effect of the local shear strain  $\gamma$ . Crosses and circles show ratios of normal stress components  $\sigma_{yy}/\sigma_{u'u'}$  and  $\sigma_{v'v'}/\sigma_{u'u'}$ , respectively. The parameter  $\alpha$  (triangles) indicate the angle between the local shear stress and shear strain.

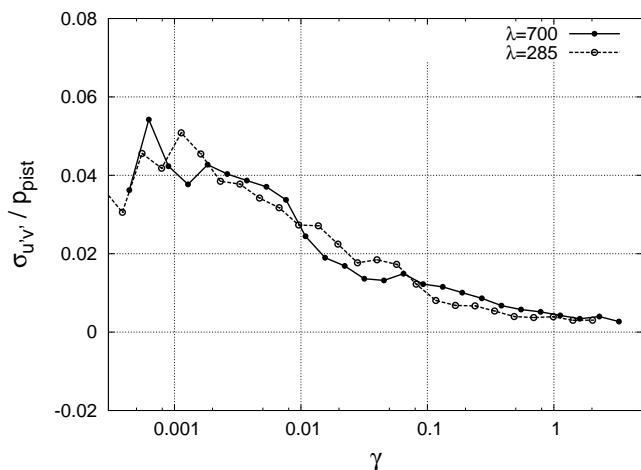


FIG. 12: The remaining shear stress  $\sigma_{u'v'}$  vanishes for large shear deformations. The open circles and dots correspond to measurements started at  $\lambda = 285$  and  $700$ , respectively. In both cases the measurement lasted over a period  $\lambda = 120$ .

#### IV. CONCLUSIONS

We studied shear flows in a linear split-bottom cell by means of computer simulations. The formation of

wide shear zones was analyzed in the presence and in the absence of gravity. In the former case pressure scales with depth, in the latter case it is approximately constant. However, in both cases the same type of wide shear zones emerge.

We showed that the widening of the shear zone in the bulk can be described by one master curve which holds for various sizes and pressure conditions. The shape of the widening function is a quarter of a circle and not a power law as was suggested before. We hope that this result will promote the development of the proper continuum theory for quasi-static flows.

We analyzed the persistent growth of the critical zone and its effect on the rheology. It influences the velocity field and the stresses, and it causes a transient of the shear zone at the beginning of the shear test.

It was shown that the form of the stress tensor becomes simpler with increasing shear strain  $\gamma$ . The region, where the stress tensor takes the reduced form (4), was also analyzed by Depken et al. [11]. The authors found that this region can be best characterized by the inertial parameter  $I$  [3] which is defined to be proportional to the shear rate  $\dot{\gamma}$  and to the inverse pressure. As it was pointed out in [11] it is not clear how the emergence of the inertial number can be reconciled with the rate independence of quasi-static flows. It is the task of future work to clarify the question what influence the parameters  $\gamma$  and  $I$  have on the stress tensor in case of slow deformations.

#### Acknowledgments

We wish to thank János Kertész for many suggestions and critical remarks, and in particular for his hospitality extended to AR during a research visit. We acknowledge partial support by grant OTKA T049403, Öveges project GranKJ06 of **KPI** and **ÖNKTH** and the G.I.F. grant No. I-795-166.10/2003. DEW thanks Francois Chevoir and Jean-Noel Roux for their hospitality and many discussions on granular rheology during the fall of 2005.

[1] I. S. Aranson and L. S. Tsimring, *Rev. Mod. Phys.* **78**, 641 (2006).  
 [2] P. G. de Gennes, *Rev. Mod. Phys.* **71**, 374 (1999).  
 [3] GDR\_MiDi, *Eur. Phys. J. E* **14**, 341 (2004).  
 [4] D. Fenistein and M. van Hecke, *Nature* **425**, 256 (2003).  
 [5] D. Fenistein, J. W. van de Meent, and M. van Hecke, *Phys. Rev. Lett.* **92**, 094301 (2004).

[6] S. Luding, in *The Physics of Granular Media* (Wiley-VCH, Weinheim, 2004), pp. 299–324.  
 [7] T. Unger, J. Török, J. Kertész, and D. E. Wolf, *Phys. Rev. Lett.* **92**, 214301 (2004), cond-mat/0401143.  
 [8] D. Fenistein, J.-W. van de Meent, and M. van Hecke, *Phys. Rev. Lett.* **96**, 118001 (2006).  
 [9] X. Cheng, J. B. Lechman, A. Fernandez-Barbero, G. S.



- Grest, H. M. Jaeger, G. S. Karczmar, M. E. Möbius, and S. R. Nagel, Phys. Rev. Lett. **96**, 038001 (2006).
- [10] M. Depken, W. van Saarloos, and M. van Hecke, Phys. Rev. E **73**, 031302 (2006).
- [11] M. Depken, J. B. Lechman, M. van Hecke, W. van Saarloos, and G. S. Grest (2006), cond-mat/0611080.
- [12] T. Unger, Phys. Rev. Lett **98**, 018301 (2007).
- [13] J. Török, T. Unger, J. Kertész, and D. E. Wolf, Phys. Rev. Lett. **75**, 011305 (2007), cond-mat/0607162.
- [14] M. Jean, Comput. Methods Appl. Mech. Engrg. **177**, 235 (1999).
- [15] L. Brendel, T. Unger, and D. E. Wolf, in *The Physics of Granular Media* (Wiley-VCH, Weinheim, 2004), pp. 325–343.
- [16] K. Rónaszegi, T. Unger, and J. Kertész (2007), to be published.
- [17] D. M. Wood, *Soil Behaviour and Critical State Soil Mechanics* (Cambridge University Press, Cambridge, 1990).
- [18] F. Radjai and S. Roux, in *The Physics of Granular Media* (Wiley-VCH, Weinheim, 2004), pp. 165–187.
- [19] R. F. Craig, *Craig's soil mechanics* (Spon Press, New York, 2004).
- [20] F. da Cruz, S. Emam, M. Prochnow, J.-N. Roux, and F. Chevoir, Phys. Rev. E **72**, 021309 (2005).
- [21] D. Kadau, D. Schwesig, J. Theuerkauf, and D. E. Wolf, Granular Matter **8**, 35 (2005).